Supporting Information

Schulz et al. 10.1073/pnas.1315858110

Theory of Image-Scanning Microscopy

Let us first shortly recall image formation in a conventional wide-field and in a confocal microscope. In a wide-field microscope with homogeneous illumination of the sample, the image $I(\mathbf{s})$, which is the intensity at pixel position $\mathbf{s}$ on the CCD of the imaging camera, is given by

$$I(\mathbf{s}) = \int d\mathbf{r}' D(\mathbf{s}-\mathbf{r}') S(\mathbf{r}'),$$

where $D(\mathbf{s}-\mathbf{r}')$ is the point-spread function (PSF) of the wide-field microscope describing the intensity generated at position $\mathbf{s}$ on the CCD by a point emitter at position $\mathbf{r}'$ in the sample, and $S(\mathbf{r}')$ is the sample function describing the density of emitters at position $\mathbf{r}'$ in the sample. Knowing the PSF, the optical transfer function (OTF) for wide-field imaging is simply the Fourier transform of $D(\mathbf{s}-\mathbf{r}')$. Here and below, we assume that the image coordinate $\mathbf{s}$ is given in normalized units corresponding to a 1:1 image magnification (back projection of the image into sample space). Without restriction of generality, this significantly simplifies all the ensuing mathematics.

The situation becomes more complex for a confocal microscope, which scans the sample with a focused laser beam and detects the fluorescence by focusing it through a confocal circular pinhole onto a point detector (avalanche photodiode or photomultiplier tube). Let the light intensity distribution in the focus be $E(\mathbf{r}-\mathbf{r}')$, which is a function of the distance between the point of interest, $\mathbf{r}'$, and the center position of the focus, $\mathbf{r}$. Then, the image of the confocal microscope is given by

$$I(\mathbf{r}) = \int d\mathbf{s} \int d\mathbf{r}' A(\mathbf{s}) D(\mathbf{s}-\mathbf{r}'+\mathbf{r}) E(\mathbf{r}-\mathbf{r}') S(\mathbf{r}').$$

Here, D and S have the same meaning as before, but $A(\mathbf{s})$ describes the action of the confocal aperture and is given by

$$A(\mathbf{s}) \equiv A(s) = \begin{cases} 1 & \text{if} \quad s < a \\ 0 & \text{if} \quad s > a \end{cases},$$

where a is the radius of the confocal aperture when back-projected into sample space. We can define the PSF $U_{con}(\mathbf{r})$ of this confocal microscope via

$$I(\mathbf{r}) = \int d\mathbf{r}' U_{con}(\mathbf{r}-\mathbf{r}') S(\mathbf{r}')$$

so that one has

$$U_{con}(\mathbf{r}) = \int d\mathbf{s} A(\mathbf{s}) D(\mathbf{s}+\mathbf{r}) E(\mathbf{r}).$$

By replacing the functions D and E by their Fourier transforms, one finds

$$U_{con}(\mathbf{r}) = \int d\mathbf{s} \int d\mathbf{k} \int d\mathbf{k}' A(\mathbf{s}) \tilde{D}(\mathbf{k}') e^{i\mathbf{k}'\cdot(\mathbf{s}+\mathbf{r})} \tilde{E}(\mathbf{k}) e^{i\mathbf{k}\cdot\mathbf{r}},$$

where a tilde here denotes the Fourier transform of the corresponding function. Now, the integration over $\mathbf{s}$ can be performed explicitly, yielding

$$\int d\mathbf{s} A(\mathbf{s}) e^{i\mathbf{k}\cdot\mathbf{s}} = \int_0^a ds s \int_0^{2\pi} d\phi e^{iqs\cos\phi} = 2\pi \int_0^a ds s J_0(qs) = \frac{2\pi a}{q} J_1(qa).$$

Here, the J_n denote Bessel functions of the first kind of order n. Thus, one finds up to a constant prefactor,

$$U_{con}(\mathbf{r}) = \int d\mathbf{k} e^{i\mathbf{k}\cdot\mathbf{r}} \left[\int d\mathbf{k}' \frac{J_1(aq')}{q'} \tilde{D}(\mathbf{k}') \tilde{E}(\mathbf{k}-\mathbf{k}') \right],$$

and correspondingly for the OTF,

$$\tilde{U}_{con}(\mathbf{k}) = \int d\mathbf{k}' \frac{J_1(aq')}{q'} \tilde{D}(\mathbf{k}') \tilde{E}(\mathbf{k}-\mathbf{k}').$$

Here, we restrict ourselves to the case that both the excitation intensity profile $E(\mathbf{r})$ and the wide-field PSF $D(\mathbf{r})$ are symmetric functions with respect to the optical axis; then, one also has $\tilde{D}(\mathbf{k}) = \tilde{D}(q,w)$ and $\tilde{E}(\mathbf{k}) = \tilde{E}(q,w)$, where q is the radial Fourier coordinate perpendicular to the optical axis and w is the axial Fourier coordinate parallel to the optical axis. In that case, one may use a Hankel transform to represent both $J_1(aq)\tilde{D}(q,w)/q$ and $\tilde{E}(q,w)$ in the form

$$\frac{J_1(aq)\tilde{D}(q,w)}{q} = \int_0^\infty d\xi\, \xi\, \tilde{\tilde{F}}(\xi,w) J_0(q\xi)$$

and

$$\tilde{E}(q,w) = \int_0^\infty d\xi\, \xi \tilde{\tilde{E}}(\xi,w) J_0(q\xi),$$

where we have introduced the Hankel transforms $\tilde{\tilde{F}}$ and $\tilde{\tilde{E}}$, which themselves are given by

$$\tilde{\tilde{F}}(\xi,w) = \int_0^\infty dq\, J_1(aq) \tilde{D}(q,w) J_0(q\xi)$$

and

$$\tilde{\tilde{E}}(\xi,w) = \int_0^\infty dq q \tilde{E}(q,w) J_0(q\xi).$$

Inserting these representations in the equation for $\tilde{U}_{con}$ yields

$$\tilde{U}_{con}(\mathbf{k}) = \int_0^\infty dq' q' \int_{-\infty}^\infty dw' \int_0^{2\pi} d\psi \int_0^\infty d\xi' \xi' \int_0^\infty d\xi \xi \tilde{\tilde{F}}(\xi',w') J_0(\xi' q') \tilde{\tilde{E}}(\xi, w-w') J_0\left(\xi\sqrt{q^2+q'^2-2qq'\cos\psi}\right).$$

Now, one may use Graf's addition theorem

$$J_0(|\mathbf{u}+\mathbf{v}|) = \sum_{n=-\infty}^{\infty} J_n(|\mathbf{u}|) J_n(|\mathbf{v}|) \cos(n\varphi)$$

where $\mathbf{u}$ and $\mathbf{v}$ are two vectors and ϕ is the angle between them. This can be used to expand the last Bessel function in the

above integral and then to perform the integration over ψ. Then one finds

$$\tilde{U}_{con}(\mathbf{k}) = \int_0^\infty dq'q' \int_{-\infty}^{\infty} dw' \int_0^\infty d\xi'\xi' \int_0^\infty d\xi\xi \tilde{\tilde{F}}(\xi', w') J_0(\xi' q') \tilde{\tilde{E}}(\xi, w - w') J_0(\xi q) J_0(\xi q').$$

Using also the orthogonality relation for Bessel functions,

$$\int_0^\infty dq\, q J_0(q\xi') J_0(q\xi) = \frac{\delta(\xi - \xi')}{\xi},$$

the expression for the OTF simplifies further to

$$\tilde{U}_{con}(q, w) = \int_{-\infty}^{\infty} dw' \int_0^\infty d\xi\xi\, \tilde{\tilde{F}}(\xi, w') \tilde{\tilde{E}}(\xi, w - w') J_0(\xi q).$$

The PSF is obtained by a Fourier–Hankel back transformation of this OTF.

In image scanning microscopy (ISM), the point detector of a conventional confocal microscope is replaced by an imaging detector so that at each scan position, an image of the illuminated region is recorded. Thus, the raw data of an ISM image have the form

$$I(\mathbf{r}, \mathbf{s}) = \int d\mathbf{r}' A(\mathbf{s}) D(\mathbf{s} - \mathbf{r}' + \mathbf{r}) E(\mathbf{r} - \mathbf{r}') S(\mathbf{r}'),$$

where **r** denotes the scan position and **s** the position on the imaging CCD. When integrating $I(\mathbf{r}, \mathbf{s})$ over **s**, one recovers the image as obtained by the confocal microscope. One also might first shift the data in **r**-space by an amount of –**s** and then integrate over **s**, which would recover the image as obtained by a pure wide-field microscope. As visualized in Fig. 1*B* in the main text, the expression $D(\mathbf{s} - \mathbf{r}' + \mathbf{r}) E(\mathbf{r} - \mathbf{r}')$ is the product of the excitation intensity distribution E with the shifted PSF for wide-field imaging (shifted by an amount –**s**). If one neglects the Stokes shift between excitation and emission wavelength so that $D(\mathbf{r}) = E(\mathbf{r})$, then the center of gravity of the product $D(\mathbf{s} - \mathbf{r}' + \mathbf{r}) E(\mathbf{r} - \mathbf{r}')$ is shifted by an amount –**s**/2 from the optical axis. The idea of ISM is to shift this center of gravity back toward the optical axis, i.e., by +**s**/2, and only then to integrate over **s**. The result is

$$I_{ISM}(\mathbf{r}) = \int d\mathbf{s}\, I\left(\mathbf{r} - \frac{\mathbf{s}}{2}, \mathbf{s}\right) = \int d\mathbf{r}' \int d\mathbf{s}\, A(\mathbf{s}) D\left(\mathbf{r} - \mathbf{r}' + \frac{\mathbf{s}}{2}\right) E\left(\mathbf{r} - \mathbf{r}' - \frac{\mathbf{s}}{2}\right) S(\mathbf{r}')$$

so that the PSF of ISM is given by

$$U_{ISM}(\mathbf{r}) = \int d\mathbf{s}\, A(\mathbf{s}) D\left(\mathbf{r} + \frac{\mathbf{s}}{2}\right) E\left(\mathbf{r} - \frac{\mathbf{s}}{2}\right).$$

This shift and integration means that light recorded at pixel position **s** with the scan focus at position **r** is added to the final image at position **r** + **s**/2. This may be done either by shrinking the CCD image taken at one scan position by a factor of two and then adding this shrunken image at center position **r** to the final image or by taking the CCD image recorded at scan position **r** as it is and then adding it at center position 2**r** to the final image. In the latter case, one has to rescale the final image by one half after the ISM procedure is completed. In our implementation of ISM with a spinning-disk confocal microscope, we use the latter option, which is much less demanding computationally and extremely simple. The implementation using Matlab is outlined in *ISM Algorithm and Image Calculation Using Matlab*.

For explicitly calculating the PSF and OTF of ISM, one again may use the axial symmetry of both D and E to reduce the 3D integral to a 2D one. First, one expresses both D and E by their Hankel transforms,

$$D(\mathbf{r}) = D(\rho, z) = \int dq\, q\, \tilde{D}(q, z) J_0(q\rho)$$

and

$$E(\mathbf{r}) = E(\rho, z) = \int dq\, q\, \tilde{E}(q, z) J_0(q\rho).$$

Again using Graf's addition theorem and integrating over **s** one finds

$$U_{ISM}(\rho, z) = 4\pi \int dqq \int dq'q'\, \tilde{D}(q, z) R(q, q', \rho) \tilde{E}(q', z),$$

where the kernel function

$$R(q, q', \rho) = \sum_{n=0}^{\infty} \frac{(-1)^n a J_n(q\rho) J_n(q'\rho) \left[q' J_n(qa/2) J_{n-1}(q'a/2) - q J_{n-1}(qa/2) J_n(q'a/2)\right]}{q^2 - q'^2}$$

was introduced, which takes, in the limit $q' \to q$, the value

$$R(q, q, \rho) = \sum_{n=0}^{\infty} \frac{(-1)^n a^2 J_n(q\rho) J_n(q'\rho) \left[J_n^2(qa/2) - J_{n-1}(qa/2) J_{n+1}(qa/2)\right]}{4}.$$

The OTF finally is obtained by a Fourier–Hankel transform of the PSF.

Finally, we have to specify the excitation intensity distribution $E(\mathbf{r})$ and the PSF of wide-field imaging $D(\mathbf{r})$. In the scalar approximation (neglecting the vector character and polarization of the electromagnetic field), the light intensity distribution generated by focusing a plane wave through a perfect objective with maximum light collection angle Θ is given by

$$E(\rho, z) \propto \left| \int_0^{\Theta} d\theta \sqrt{\cos\theta} \sin\theta \exp(ikz\cos\theta) J_0(k\rho\sin\theta) \right|^2,$$

where $k = 2\pi n/\lambda$ is the wave number of light with vacuum wavelength λ inside the objective's immersion medium of refractive index n. As already mentioned above, under ideal conditions and while neglecting any Stokes shift between excitation and detection wavelengths, the PSF for wide-field imaging $D(\mathbf{r})$ is identical to $E(\mathbf{r})$.

We performed numerical calculations for an excitation (detection) wavelength of 500 nm, assuming a confocal pinhole diameter of 500 nm (back projection in sample space), and a maximum angle of light collection and focusing corresponding to a numerical aperture of the objective of 1.2 and a refractive index of the objective's immersion medium of 1.33 (water). Fig. S1 compares the resulting OTFs for a wide-field microscope, the conventional confocal microscope, and the ISM microscope with pinhole. The green solid line denotes the limits of the support of the maximally extended OTF, which is obtained by an autoconvolution of the OTF of the wide-field microscope, which corresponds to the support of the OTF of a hypothetical confocal microscope with zero-size pinhole. This also is the maximum possible support an OTF can have for any diffraction-limited optical microscope.

Fourier Reweighting

Although the OTF of an ISM nearly completely fills the whole frequency range maximally accessible by a diffraction-limited microscope, the amplitude distribution of its OTF is not optimal. We will demonstrate this by a simplified discussion of the imaging properties of ISM for objects within the focal plane of the microscope. In this case, we assume that the confocal aperture of the microscope does not significantly restrict light detection laterally, i.e., perpendicular to the optical axis, so that the PSF of an ISM simplifies to

$$U_{ISM}(\boldsymbol{\rho}) \approx \int d\mathbf{s}\, D\left(\boldsymbol{\rho} + \frac{\mathbf{s}}{2}\right) E\left(\boldsymbol{\rho} - \frac{\mathbf{s}}{2}\right),$$

where $\boldsymbol{\rho}$ is the lateral scan position perpendicular to the optical axis (i.e., here we strictly consider imaging from the focal plane of the objective into the conjugate plane of the CCD). Thus, we assume that the excitation intensity distribution (as well as the wide-field imaging PSF) has fallen off to negligible values before the presence of the confocal aperture makes itself tangible. This approximation tremendously simplifies the (lateral) OTF of the ISM system, which now reads

$$\tilde{U}_{ISM}(\mathbf{q}) \approx \tilde{D}\left(\frac{\mathbf{q}}{2}\right)\tilde{E}\left(\frac{\mathbf{q}}{2}\right) \approx \tilde{D}^2\left(\frac{\mathbf{q}}{2}\right).$$

From this expression, it clearly is visible that the support of the OTF of an ISM is approximately twice as large as the support of the original wide-field PSF (or of the Fourier transform of excitation intensity distribution), which signifies a doubled lateral resolution. However, the ideal OTF for a microscope with doubled resolution would not be $\tilde{D}^2(\mathbf{q}/2)$ but $\tilde{D}(\mathbf{q}/2)$. Thus, the OTF of an ISM overweighs components of the OTF with large amplitude (small values of $|\mathbf{q}|$) and underweighs components with small amplitude (large values of $|\mathbf{q}|$). A naïve approach would be to reweigh the Fourier transform of an obtained ISM image with the weight function $\tilde{D}^{-1}(\mathbf{q}/2)$, which, however, is dangerous because $\tilde{D}(\mathbf{q})$ falls off to zero toward the edge of its support. Thus, we instead use as a weight function

$$\tilde{W}(\mathbf{q}) = \frac{1}{\tilde{D}(\mathbf{q}/2) + \varepsilon}$$

with a small normalizing parameter ε, which should be by one order or more smaller than the maximum amplitude of $|\tilde{D}(\mathbf{q})|$. This prevents the amplification of image noise at high frequencies in Fourier space. Fig. S2 compares the PSFs of the wide-field microscope, the confocal microscope, and the Fourier-reweighted ISM, demonstrating the reduction in extent of the PSF from wide-field microscope to ISM. The $1/e^2$ widths of the three distributions are 222 nm for the wide-field microscope, 198 nm for the confocal microscope, and 128 nm for the ISM with Fourier reweighting.

ISM Algorithm and Image Calculation Using Matlab

The data recorded in one-focus ISM as described in ref. 1 are four-dimensional: at each position of the scan–focus, one records a 2D image of the illuminated region so that one finally obtains data depending on both the relative position of the focus in the sample and the 2D pixel positions on the camera. Then, to calculate the ISM image, one shifts each pixel halfway toward the optical before registering it at the current scan position. In confocal spinning-disk ISM (CSD-ISM), however, there are multiple scanning foci corresponding to the microlenses and pinholes in the Nipkow disk. Before we can apply the pixel reassignment of the ISM data, we need to know their position. This is achieved by imaging a uniformly fluorescing sample in ISM mode (stroboscopic illumination). Then, for each image in a sequence, the position of the spots is determined using the rapidSTORM software (version 3.2) (2).

After finding the center positions of the foci for each frame, a Matlab script is used to calculate the ISM image from the raw data. First, the coordinates of the foci are loaded and adjusted to an image size that in both dimensions is 10 times that of the final ISM image. Enlarging the image matrix in this fashion accounts for the fact that the focus centers are not necessarily in the center of a pixel. Now, for every frame in the sequence, and for every focus position in the image, the raw data from a square area around the pinhole coordinate are copied to the final image matrix at a position with the coordinates multiplied by two. This procedure corresponds to moving the information from each pixel half its distance to the optical axis. The size of the area from which the data are taken (window) is three times the width of a Gaussian fit to a spot in the reference data, or in Matlab code:

```
Final_image(2*yc + window, 2*xc + window)
= Final_image(2*yc + window, 2*xc + window)
+ ((raw_data(yc + window, xc + window)) - background).
```

Here, the indices for number of image and pinhole position have been omitted; xc and yc are the pinhole coordinates; and background is the readout noise of the camera. If the position of the pinhole is too close to the edge of the image, such that the square from which data are taken would be outside the image, it is discarded. After summing over all images and pinhole positions, the final image is reduced by a factor of 10. On this final image, the Fourier reweighting as described before is performed.

A CSD-ISM image calculation plugin for ImageJ may be found on our Web site (www.joerg-enderlein.de/ISM).

Synchronization and Data Acquisition

The core of the CSD microscope is composed of two rapidly and synchronously rotating disks, one with an array of microlenses and the other with a coaligned array of pinholes. These microlenses and pinholes are arranged in Archimedean spirals (Nipkow disk geometry), and repeat every 1/12th of disk rotation. The spin-disk unit is operated at a speed of 1,500 rpm so that the same focal spot arrangement repeats itself 300 times per second. At this speed, the laser pulses used for the stroboscopic illumination have to be short enough so that any elongation of the foci becomes negligible. We have chosen a pulse length of 6 μs because at about 8 μs pulse length, focal spot asymmetry becomes discernible. The microlenses/pinholes on the spin disk are relatively far apart to prevent excessive cross-talk between focal spots during image acquisition (detection of fluorescence excited in one focus through a pinhole associated with another focus). However, because we use stroboscopic illumination, we can increase the number of apparent spots by illuminating the sample more than once during one repetition period of the focal spot arrangement. For synchronizing the laser pulsing with the spin-disk rotation, we use the trigger signals generated by the spin-disk unit. A long trigger marks a full rotation of the disk, whereas 11 shorter triggers mark each additional image frame. The movement of the spin disk, the laser pulses, and the exposure of the camera are coordinated via a field-programmable gate array (FPGA; NI PCIe-7842R; National Instruments). The programming of the FPGA is realized using LabVIEW. As the disk rotates, the time T between each trigger is calculated. This time is used to calculate the laser trigger signals for the next frame. Explicitly, in cycle number n + 1, the period T(n) is divided into four equal parts to produce laser pulses at times 0, T(n)/4, T(n)/2, 3*T(n)/4 after the spin-disk trigger. In the next cycle, these times are augmented by a certain delay that, in effect, moves the focus pattern. The delays are calculated by dividing T(n) into 1,000 equal parts (Fig. S3). Using four pulses in one cycle, this corresponds to 250 steps for one full image acquisition. The camera exposure is triggered in synchronization with the laser pulses. The camera trigger is produced shortly after the last laser trigger in a cycle so that the readout sequence, which is at the beginning of a frame (frame transfer mode), is finished when the first laser pulse of a cycle starts. Using the four-pulse sequence, one full ISM image (250 steps) can be acquired within 1 s.

In addition to the 4-pulse sequence, a 16-pulse sequence may be used. An 8-pulse sequence is generated in a manner similar to that of the 4-pulse sequence, and it is duplicated by introducing a short delay (20 μs) to the triggers. In this illumination scheme, 125 images are used to create one full image within 0.5 s. However, for the 8- and 16-pulse sequences, the images of the foci start to overlap, causing slight artifacts in the final ISM image. Thus, using the 16-point illumination is a tradeoff between speed and image quality. In the Fourier reweighted image, however, the artifacts often are reduced and may be eliminated by Fourier filtering, with no obvious loss of information in the image.

The distance between spots of consecutive steps of the sequence is about 100 nm for a 250-image sequence (125-image sequence for 8- or 16-pulse sequences). The y distance between spots (after the next row is at the same x position) is about 66 nm (about 33 nm with 8- or 16-pulse sequence).

The camera trigger may be set to occur less frequently than once for every laser pulse sequence. In effect, the recording speed may be matched to the camera frame rate for larger areas of interest or to allow for a longer accumulation of light for obtaining a better signal-to-noise ratio. For most images recorded, the camera was triggered after 23 laser pulse cycles, corresponding to an acquisition time of 20 s for 250 images in a sequence. For all images recorded, the software waited for one trigger from the spin disk before starting the next cycle.

Because the triggers for both the laser and the camera are produced by the FPGA, which depends only on the input of the spin-disk trigger, the camera's operation does not depend on the use of special acquisition software; homemade solutions, as well as the manufacturer's control software, may be used. For data acquisition, we used a custom-made LabVIEW program, but we also tested the functionality of the spin-disk ISM using Andor's Solis software (*CSD-ISM with an sCMOS Camera*).

The four-pulse illumination sequence also may be used to introduce simultaneous multicolor imaging by routing the pulse trigger to four different lasers. In this fashion, the fluorescence excited by the different excitation wavelengths will be well separated on the camera chip. Because the CSD is synchronized with the lasers, the emission of a certain color will always appear on the same spot of the camera for a given image in the sequence. Taking reference data for each color individually, the data may be sorted and analyzed separately.

Signal Strength and Signal-to-Noise Ratio

To achieve the stroboscopic illumination, the laser pulses must be very short. In the case of a rotation of the disk at 1,500 rpm (12 images per full rotation, 300 images per second), we used a laser pulse length of 6 μs. This means that we effectively illuminated only about 1/555 of the time vs. continuous illumination. (This fraction does not change for faster rotation of the disk because in this case, the laser pulse length also has to be shortened to maintain the size of the foci.) For a sequence of 250 images, which may be calculated into the final ISM image, this means that the ISM image would be about 2.2 times dimmer than the fastest possible regular spinning-disk image (3.3 ms per frame). However, by using the four-pulse sequence, the shortest-acquisition-time ISM image is about 1.8 times brighter than the fastest possible spinning-disk image. For the Tau protein measurements (see Fast 3D Imaging of Tau Protein in the main text), the 16-pulse sequence was used, which increases the brightness by another factor of four. This means that within 1 s, an image about seven times brighter than the fastest possible regular CSD image can be recorded.

An important question is the signal-to-noise ratio of CSD-ISM in comparison with normal wide-field microscopy and structured illumination microscopy (SIM). Here, we refer to the work by Pitter and coworkers (3–5), who have given an excellent analysis of the impact of photon detection noise on the frequency spectrum of the OTF of various types of microscopes. In their publications, they show that a SIM system shows optimal performance in terms of signal-to-noise ratio across the Fourier spectrum of the OTF. In comparison, ISM is equivalent to a confocal microscope with infinitely small pinhole, which has a suboptimal signal-to noise ratio at larger spatial frequencies; see the detailed analysis and figures (especially figure 2) in ref. 3. The reason is that in SIM, the excitation intensity is modulated with the largest possible spatial frequency, whereas the laser focus of a confocal laser scanning system is a superposition of all possible spatial frequencies, leading to an overweighting of lower frequencies with respect to higher spatial frequencies. Thus, SIM shows a better signal-to-noise performance than ISM, but at the price of much higher technical complexity.

CSD-ISM with an sCMOS Camera

For most experiments, we chose the EM CCD over the sCMOS camera based on its superior sensitivity. The larger chip of the sCMOS, however, allows us to image the whole area illuminated by the CSD. For fixed samples, for which fast imaging is not crucial, one may integrate over many laser pulse cycles to get a better signal-to-noise ratio. Readout noise and the varying intensity-to-signal performance of every pixel were taken into account by subtracting a background image from each image of the ISM raw data stack. With our Neo sCMOS (2,560 × 2,160 pixels^2, 6.5-μm pixel size; Andor Technology), the area illumi-

nated by the spin disk corresponded to 2,048 × 1,461 pixels^2, or 111 × 79 μm^2. The data acquisition was performed using Andor Solis software in the "external exposure" trigger mode. In this fashion, data were gathered at all times between two camera triggers.

Fig. S5 shows a three-color confocal and ISM image of a cell with labeled actin (Alexa 488, blue), tubulin (Alexa 568, green), and paxillin (Alexa 647, red). The sample is the same as that described in the main text. Each image of the ISM raw data were averaged over 35 or 95 laser pulse sequences for 488 nm or 561/647 nm excitation, respectively, to achieve a good signal-to-noise ratio.

Fast 3D Imaging of Tau Protein

Movie S1 shows 3D projections of CSD data (*Upper*) and CSD-ISM data (*Lower*) of Tau protein aggregates, both processed with 3D deconvolution.

Three-dimensional deconvolution of *z*-stack data were performed using Piotr Wendykier's ImageJ plugin: https://sites.google.com/site/piotrwendykier/software/deconvolution/paralleliterativedeconvolution.

For deconvolution, we used the ISM data before Fourier reweighting and a theoretical ISM PSF, obtained by stretching the Fourier components of the 2D wide-field PSF by a factor of two, as described in *Fourier Reweighting*. The 3D PSF is composed of 31 2D PSFs for different focus positions separated by 100 nm. The settings for the deconvolution were Wiener Filter Preconditioned Landweber (WPL), Reflexive, Auto, Same as source, Double, and Max 10–50 iterations. The WPL options were Normalize PSF, Perform anti-ringing step, Detect divergence, Gamma 0, Low pass 1, and Termination 0.01.

Four-Color 3D Imaging

Fig. S4 shows a confocal image of a cell and the CSD-ISM image after 3D deconvolution of the same cell. Details on the sample preparation may be found in the main text. A movie of 3D projections of this cell is available as Movie S2.

Measurement of Nuclear Pore Complex Density

Nuclear pore density was measured with the ITCN ImageJ plugin, as described in *Methods*. An example of the performance of the ImageJ plugin with conventional spin disk and with ISM data is shown in Fig. S6. The region of interest in which nuclear pore complexes (NPCs) are detected is shown as a yellow oval in the upper panel. The NPCs found by the plugin are marked in red in the lower panel. Manually added NPC locations are marked in black.

1. Müller CB, Enderlein J (2010) Image scanning microscopy. *Phys Rev Lett* 104(19):198101.
2. Wolter S, et al. (2010) Real-time computation of subdiffraction-resolution fluorescence images. *J Microsc* 237(1):12–22.
3. Somekh MG, Hsu K, Pitter MC (2008) Resolution in structured illumination microscopy: A probabilistic approach. *J Opt Soc Am A Opt Image Sci Vis* 25(6):1319–1329.
4. Hsu K, Somekh MG, Pitter MC (2009) Stochastic transfer function: Application to fluorescence microscopy. *J Opt Soc Am A Opt Image Sci Vis* 26(7):1622–1629.
5. Somekh MG, Hsu K, Pitter MC (2009) Stochastic transfer function for structured illumination microscopy. *J Opt Soc Am A Opt Image Sci Vis* 26(7):1630–1637.

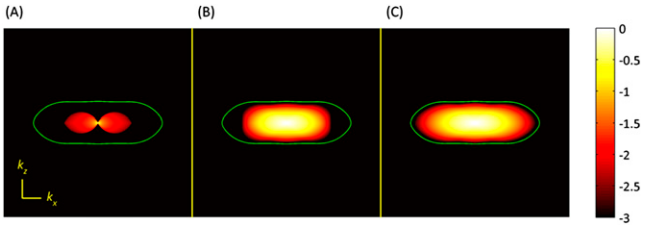

Fig. S1. Comparison of the OTFs of a wide-field microscope (*A*), a confocal microscope (*B*), and an ISM (*C*). The solid line delimits the region of maximally possible support of an optical diffraction-limited microscope. The direction of k_z is along the optical axis; the direction of k_x is perpendicular to the optical axis. The color scale gives the decadic logarithm of the normalized OTFs. The full 3D OTFs are obtained by rotating the figures shown around the optical axis.

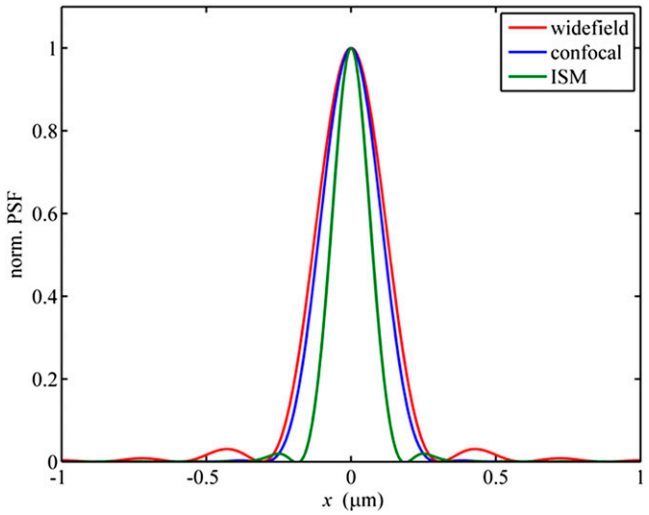

Fig. S2. Comparison of the lateral cross-sections of the PSF of a wide-field microscope, a confocal microscope, and an ISM microscope. The PSF of ISM is calculated after Fourier reweighting of its OTF, as described in the text.

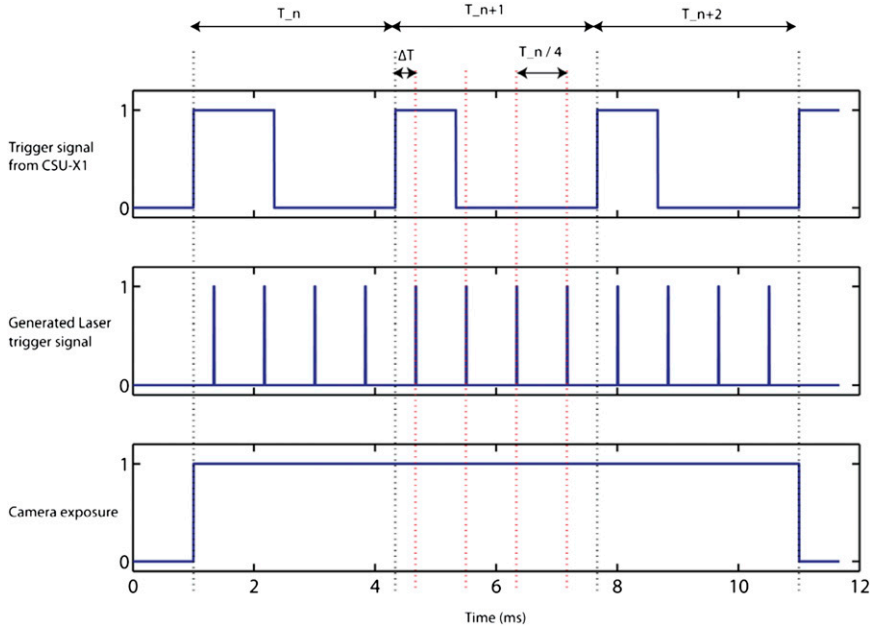

Fig. S3. Generation of trigger signals for CSD-ISM. See *Synchronization and Data Acquisition* for details.

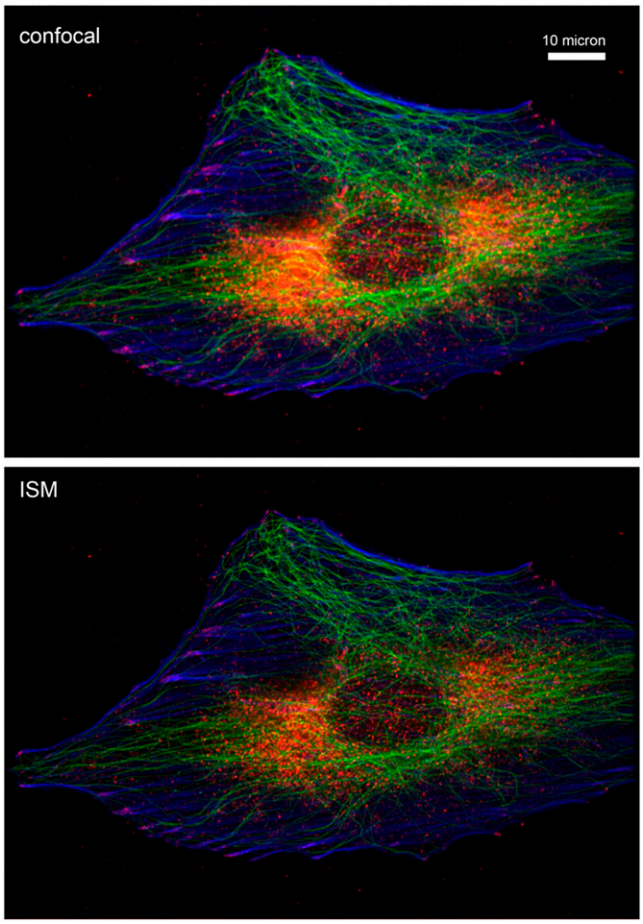

Fig. S4. sCMOS CSD-ISM images of a multicolor labeled HeLa cell. See *CSD-ISM with an sCMOS Camera* for details.

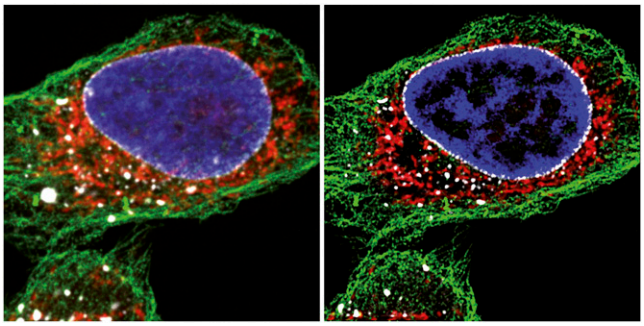

Fig. S5. HeLa P4 cell, as described in the main text. The cells were stained with Hoechst 33258 (blue) and MitoTracker M-7510 (red). α-Tubulin (green) and Nup358 (white) were detected by using specific antibodies and were visualized using Alexa 488- and Alexa 633-coupled secondary antibodies, respectively. (*Left*) CSD image; (*Right*) CSD-ISM image after 3D deconvolution using a theoretical ISM PSF. The image size is 33 μm.

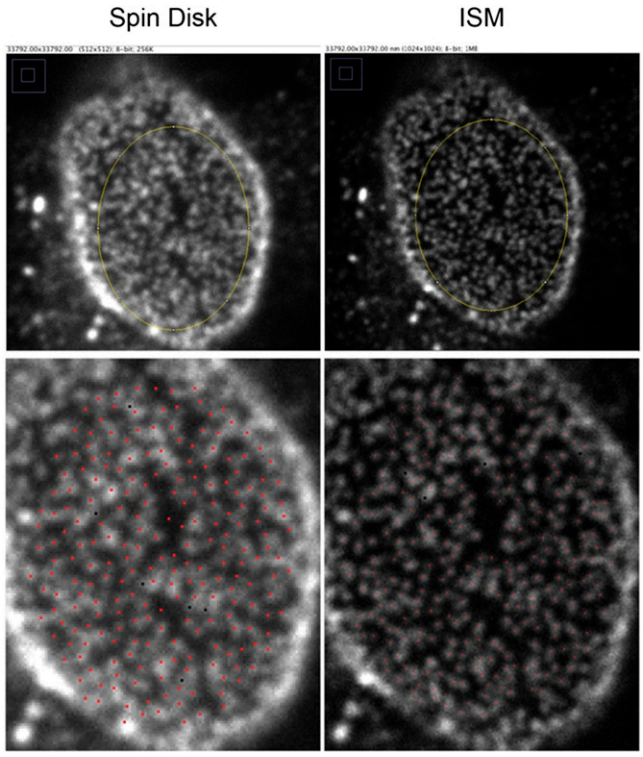

Fig. S6. Automated counting of NPCs on the nuclear membrane. (*Upper*) Region of interest used for the counting plugin. (*Bottom*) Red dots are found by the ImageJ plugin; black dots were added manually.

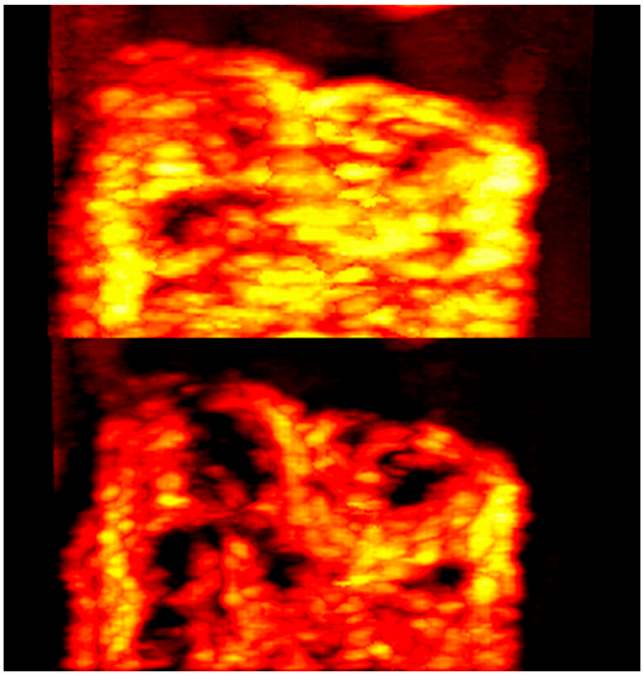

Movie S1. Three-dimensional projections of CSD data (*Upper*) and CSD-ISM data (*Lower*) of Tau protein aggregates, both processed with 3D deconvolution. Each of the 85 CSD-ISM images in the stack was acquired within 1 s. The distance between slices is 200 nm. For details, see Fast 3D Imaging of Tau Protein in the main text.

Movie S1

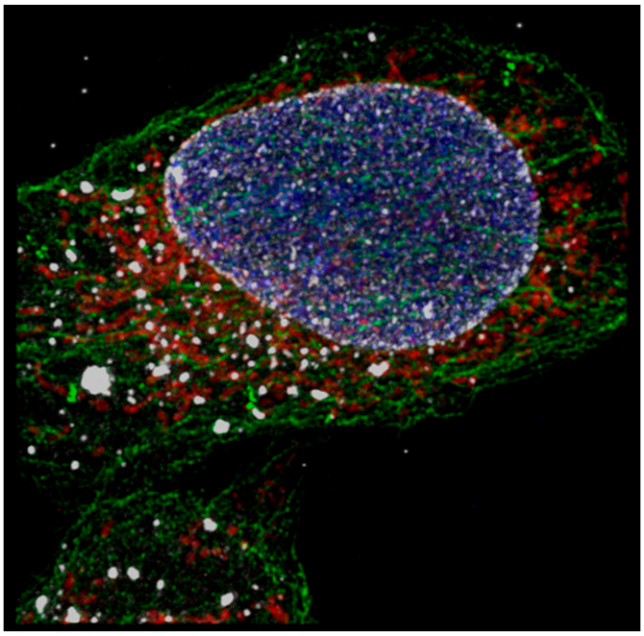

Movie S2. Three-dimensional projections of a four-color labeled cell as described in the main text. The distance between slices is 100 nm. The data were processed using 3D deconvolution.

Movie S2